Journal of Asian Earth Sciences 93 (2014) 288–300

Contents lists available at ScienceDirect

Journal of Asian Earth Sciences

journal homepage: www.elsevier.com/locate/jseaes

Source characteristics of the ~2.5 Ga Wangjiazhuang Banded Iron Formation from the Wutai greenstone belt in the North China Craton: Evidence from neodymium isotopes

Changle Wang [a,b], Lianchang Zhang [a,*], Yanpei Dai [a,b], Wenjun Li [a]

[a] Key Laboratory of Mineral Resources, Institute of Geology and Geophysics, Chinese Academy of Sciences, Beijing 100029, China
[b] University of Chinese Academy of Sciences, Beijing 100049, China

ARTICLE INFO

Article history:
Received 28 January 2014
Received in revised form 24 July 2014
Accepted 25 July 2014
Available online 5 August 2014

Keywords:
Wutai greenstone belt (WGB)
Neoarchean
Wangjiazhuang BIF
Neodymium isotopes
North China Craton (NCC)

ABSTRACT

Here we first present samarium (Sm)–neodymium (Nd) isotopic data for the ~2.5 Ga Wangjiazhuang BIF and associated lithologies from the Wutai greenstone belt (WGB) in the North China Craton. Previous geochemical data of the BIF indicate that there are three decoupled end members controlling REE compositions: high-T hydrothermal fluids, ambient seawater and terrigenous contaminants. Clastic meta-sediment samples were collected for major and trace elements studies in an attempt to well constrain the nature of detrital components of the BIF. Fractionated light rare earth elements patterns and mild negative Eu anomalies in the majority of these meta-sedimentary samples point toward felsic source rocks. Moreover, the relatively low Th/Sc ratios and positive $\varepsilon_{Nd}(t)$ values are similar to those of the ~2.5 Ga granitoids, TTG gneisses and felsic volcanics in the WGB, further indicating that they are derived from less differentiated terranes. Low Chemical Index of Weathering (CIW) values and features in the A-CN-K diagrams for these meta-sediments imply a low degree of source weathering. Sm–Nd isotopes of the chemically pure BIF samples are characterized by negative $\varepsilon_{Nd}(t)$ values, whereas Al-rich BIF samples possess consistently positive $\varepsilon_{Nd}(t)$ features. Significantly, the associated supracrustal rocks in the study area have positive $\varepsilon_{Nd}(t)$ values. Taken together, these isotopic data also point to three REE sources controlling the back-arc basin depositional environment of the BIF, the first being seafloor-vented hydrothermal fluids ($\varepsilon_{Nd}(t) < -2.5$) derived from interaction with the underlying old continental crust, the second being ambient seawater which reached its composition by erosion of parts of the depleted landmass (likely the arc) ($\varepsilon_{Nd}(t) > 0$), the third being syndepositional detritus that received their features by weathering of a nearby depleted source (likely the arc) ($\varepsilon_{Nd}(t) > 0$).

1. Introduction

Banded Iron Formations (BIFs) are chemical sedimentary rocks that precipitated throughout the Archean and early Paleoproterozoic (James, 1954; Trendall, 2002; Bekker et al., 2010). The patterns of trace element and isotopic abundances preserved in the BIFs offer a chance to infer the chemical composition and oxidation state of ancient seawater. In modern marine waters, the variation in REE+Y distributions is dominated by vary degrees of carbonate complexation and hydroxides precipitation, with REE+Y principally sourced from weathering of continents (Frei and Polat, 2007; Alexander et al., 2008), whereas, this may not have been the case in early oceans. Numerous studies on ancient BIFs indicate that hydrothermal solutions were the main source for REE and the excess of Eu in Archean seawater (e.g., Derry and Jacobsen, 1990; Shimizu et al., 1990; among others).

However, whether or not components of the BIFs were derived from continental sources, or had its origin in hydrothermal alteration of the oceanic crust has been a long-standing debate. Positive Eu anomalies are widely considered to indicate that REE in the BIFs had dominantly high-T (>350 °C) hydrothermal sources (Michard, 1989; Bau and Dulski, 1996, 1999). The high-T fluids are discharged from basaltic, mid-ocean ridge sources. Neodymium (Nd) isotopes have also been used to trace the continental vs. hydrothermal input to the BIFs (Derry and Jacobsen, 1990; Danielson et al., 1992; Bau et al., 1997). Generally speaking, the mantle-type Nd ($\varepsilon_{Nd}(t) > 0$) was often considered to represent the hydrothermal component derived from high-temperature basalt alteration, whereas the continental-type Nd ($\varepsilon_{Nd}(t) < 0$) was thought to

* Corresponding author. Tel.: +86 10 82998185; fax: +86 10 62010846.
E-mail address: lczhang@mail.iggcas.ac.cn (L. Zhang).

http://dx.doi.org/10.1016/j.jseaes.2014.07.038
1367-9120/

represent the riverine/aeolian input from weathering of continental crusts.

The North China Craton (NCC) in China hosts large amounts of ~2.5 Ga Algoma-type BIFs within the Anshan-Benxi, eastern Hebei, Wutai areas (Zhang et al., 2012; Zhai and Santosh, 2013). The Wutai greenstone belt (WGB), as the best preserved granite–greenstone terrane, is situated in the central part of the NCC (Fig. 1a) (Bai, 1986). The WGB consists of a sequence of metamorphosed ultramafic to felsic volcanic rocks, variably deformed granitoid rocks, along with lesser amounts of siliciclastic and carbonate rocks and BIFs. The distribution of REE and Y in these BIFs has been described previously (Li, 2008; Li et al., 2010; Zhang et al., 2010; Wang et al., 2014) and some significant information about the source of the BIF components have also been acquired. In summary, these BIFs show striking geochemical similarities, that are positive La, Eu and Y anomalies, a relative depletion of LREE and MREE relative to HREE, and superchondritic Y/Ho ratios (>26). These characteristics suggest that the primary chemical precipitate is a result of solutions that represent mixtures of ambient seawater and high-T hydrothermal fluids. However, considerably less information is available on the Nd isotopic compositions of these BIFs and other BIFs in China. In this regard, we report first Sm–Nd isotopic data for samples from the Wangjiazhuang BIF in the Wutai Group. In addition, we also present the Sm–Nd isotopic data for associated lithologies, including meta-basalts, meta-felsic volcanic rocks and meta-pelites. Major and trace elements whole-rock geochemical analyses of meta-pelites have also been included in order to draw an interpretation of their provenance. Combining with relevant geological background and previous geochemical data (Zhang et al., 2010; Wang et al., 2014), we can gain a comprehensive understanding of source characteristics of the BIF and additional insight into the complex depositional mechanism of the BIF.

2. Geological setting

The Hengshan–Wutai–Fuping belt is located in the middle segment of the Trans-North China Orogen (TNCO) (Fig. 1a) and consists of three distinct tectonic complexes: the upper amphibolite to granulite facies Fuping and Hengshan complexes in the southeast and northwest, respectively, separated by the greenschist- to lower amphibolite-facies Wutai Complex (Fig. 1b), which is interpreted as a typical granite–greenstone belt (Bai, 1986; Tian, 1991; Bai et al., 1992). The WGB consists of Neoarchean to Paleoproterozoic granitic plutons and metamorphosed volcanic and sedimentary rocks, traditionally named the Wutai and Hutuo Groups in the Chinese literature (Bai et al., 1992; Zhao et al., 2007). Based on lithologies and metamorphic grades, the Wutai Group is subdivided into three subgroups: Shizui, Taihuai and Gaofan subgroups (Fig. 2). The Shizui Subgroup is composed of peridotite, oceanic tholeiite, dacite, rhyolite, chert, BIFs, sandstone, siltstone and

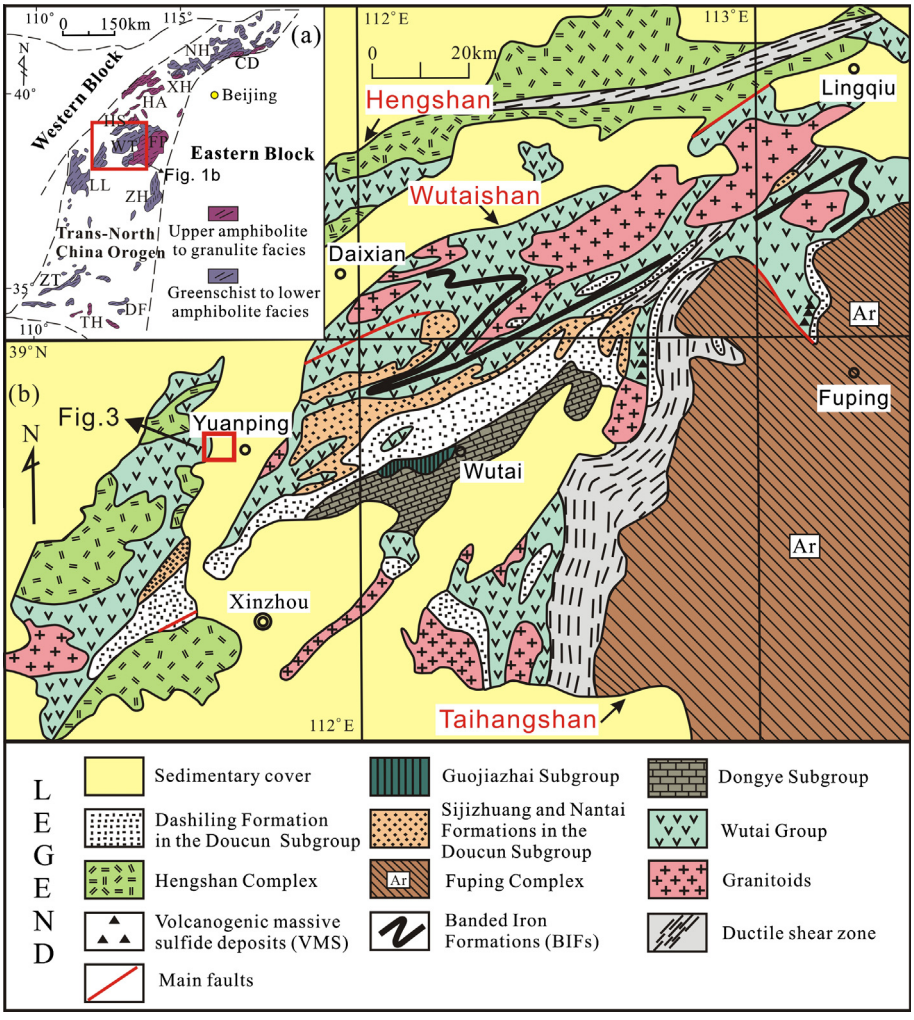

Fig. 1. (a) Regional geological sketch showing the location of the Hengshan–Wutai–Fuping belt in the North China Craton (revised after Zhao et al., 2005). Abbreviations for metamorphic complexes: CD, Chengde; DF, Dengfeng; FP, Fuping; HA, Huai'an; HS, Hengshan; LL, Lüliang; NH, Northern Hebei; TH, Taihua; WT, Wutai; XH, Xuanhua; ZH, Zanhuang; ZT, Zhongtiao. (b) Geological map of the Wutai greenstone belt (modified after Niu and Li, 2006).

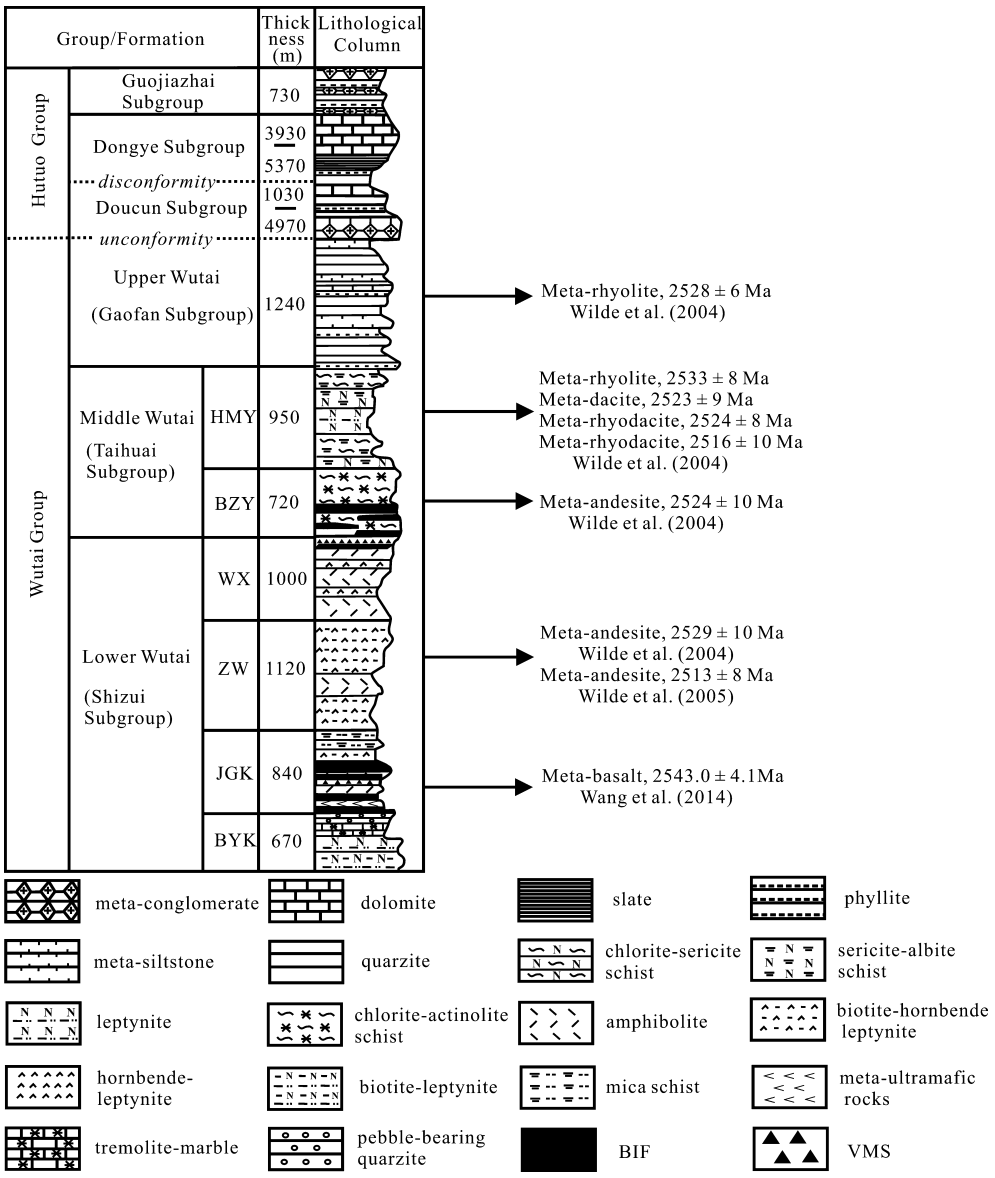

Fig. 2. Stratigraphic column showing Group and formation names for different rock assemblages in the Wutai greenstone belt (modified after Kusky and Li, 2003). Abbreviations for formation names: BYK, Banyukou Formation; JGK Jingangku Formation; ZW, Zhuangwang Formation; WX, Wenxi Formation; BZY, Baizhiyan Formation; HMY, Hongmenyan Formation.

minor limestone metamorphosed in amphibolite facies (Zhao et al., 2007). The Wangjiazhuang BIF, as one of representative BIFs in the Wutai Group, is located in the lower part of the Jingangku Formation in the Shizui Subgroup.

The Wangjiazhuang BIF is distributed nearly in a E–W direction, extending 8 km in length and 0.5 km in width, and dips to the SE with a steep angle of 60–80° (Fig. 3). Most of the BIF is deformed and primary layering is extensively transposed into a new tectonic layering or extended parallel to the plunge of the regionally dominant folds and associated lineations (Fig. 3). Laminations of the BIF have a width of ca. 7–10 mm, with greater thickness occurring in the Shenyanhe area due to tight homoclinal folding. Amphibolites were identified as meta-basalts intercalated with the Wangjiazhuang BIF, and other associated rocks include meta-felsic volcanic rocks (leptynite), metapelites (mica schist). Zhao et al. (1999) suggested that the Wutai amphibolites have undergone four metamorphic stages on the basis of petrological evidence, and the peak P–T conditions for amphibolites were estimated at 10–12 kbar and 600–650 °C. Qian et al. (2013) proposed a clockwise P–T path for the mica schist, with a peak pressure of >9.0 kbar at 615–645 °C and a peak temperature of 660 °C at ~7.5 kbar.

The Wangjiazhuang BIF is found interbedded with meta-basalts (amphibolites). Based on previous SIMS zircon U–Pb analyses of these meta-basalts, they were formed at ~2.54 Ga, representing the formation age of the Wangjiazhuang BIF (Wang et al., 2014). This zircon age reveals no difference among volcanic rocks occupying different stratigraphic levels within the Wutai Group (seen from Fig. 2). The age of the Wutai Group was previously constrained by SHRIMP zircon dating of the meta-intermediate and felsic volcanic rocks at ~2530–2515 Ma (Wilde et al., 2004, 2005).

3. Sample description and analytical methods

All samples are collected from the least altered and deformed outcrops, including bulk-BIF samples and associated rocks (amphibolites, leptynite, mica schist). These samples were

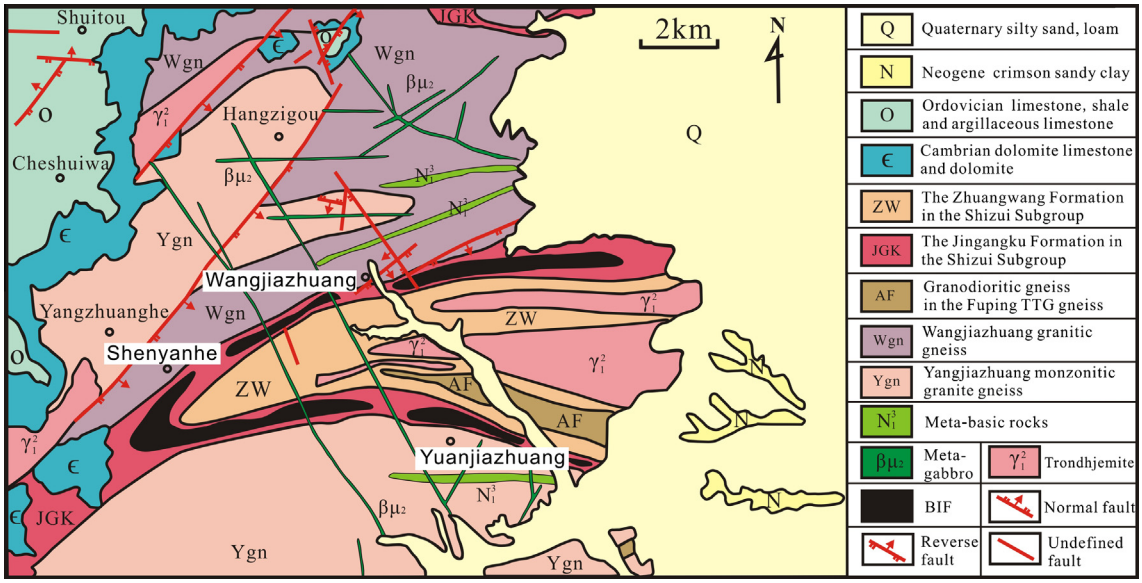

Fig. 3. Geological map of the Wangjiazhuang BIF (modified after Li, 2008).

described in detail by Wang et al. (2014) who also obtained their geochemical characteristics. Amphibolites usually exhibit a moderate- to weakly developed foliation and, in some instances, a mineral lineation (Fig. 4a). They are composed predominantly of amphibole (60–65%), plagioclase (25–30%), and lesser amounts of quartz (<5%) and biotite (<5%). Leptynites are typically dark grey, and display a fine-grained lepido-granoblastic texture and weakly developed foliation (Fig. 4b), whereas mica schist displays strong schistosity and comprises quartz (35–45%), biotite (15–20%), muscovite (15–20%), feldspar (15–20%), and minor garnet (<5%) (Fig. 4c). The poikiloblastic garnet (up to 2.5 mm) contains inhomogeneously distributed quartz, biotite and opaque mineral inclusions (Fig. 4d). The iron formation consists of alternating fine-grained Fe-rich and Si-rich micro- and mesobands ranging from less than 1 mm to 4 mm in width (Fig. 4e). The iron-rich bands are black, highly magnetic, whereas the Si-rich bands are white and generally finely laminated with a few bands of magnetite. The mineralogy of the Wangjiazhuang BIF varies both in contents and proportions. The modal mineral abundances are quartz (40–50%), magnetite (20–30%), amphibole (25–30%), minor garnet (1–5%), calcite (<2%) and pyrite (<1%) (Fig. 4f).

Geochemical analyses of meta-pelites were conducted at the Institute of Geology and Geophysics, Chinese Academy of Sciences in Beijing. Major element oxides were analyzed using XRF-1500 X-ray fluorescence (XRF) with RSD between 0.1% and 1%. Trace element concentrations were analyzed with an inductively coupled plasma-mass spectrometer (ICP-MS) (Element, Finnigan MAT) using solution methods. The accuracy on the measured concentrations is within 5–10%.

Nd isotope compositions of the BIF and associated rock samples were also determined at the Institute of Geology and Geophysics, Chinese Academy of Sciences. About 150–300 mg of powder was weighed into 7 ml SavillexTM Teflon beakers, and appropriate amounts of mixed 149Sm–150Nd spikes were added. The samples were dissolved using a mixed acid of 2 ml HF and 0.2 ml $HClO_4$ on a hotplate at 120 °C for more than 1 week. After the samples were completely dissolved, the solutions were dried on hotplate at 130–180 °C to remove the HF and $HClO_4$. The sample residues were re-dissolved in 4 ml of 6 M HCl, and then dried down again. Finally, the samples were dissolved in 5 ml of 3 M HCl. The procedures for chemical separation and isotopic measurement followed Chu et al. (2009).

The Sm–Nd isotopic analyses were conducted using a Finnigan MAT 262 thermal ionization mass spectrometer. Measured $^{143}Nd/^{144}Nd$ ratios were corrected for mass-fractionation using $^{146}Nd/^{144}Nd = 0.7219$. During the period of data collection, the measured values for the JNdi-1 Nd standard was $^{143}Nd/^{144}Nd = 0.512113 \pm 11$ (2σ, $n = 4$). The USGS reference material BCR-2 was measured for Sm–Nd isotopic composition to monitor the accuracy of the analytical procedures.

The age used for calculating the initial $^{143}Nd/^{144}Nd$ values was the U–Pb zircon age of 2543 ± 4 Ma obtained by Wang et al. (2014) for the interbedded amphibolites. T_{DM} ages were calculated according to DePaolo (1981).

4. Results

4.1. Major and trace elements

Whole-rock major, trace and REE element compositions of representative samples from the meta-pelites are given in Table 1. Table 1 also presents a compilation of reported data for the meta-pelites (Zhang et al., 2010; Wang et al., 2014). These data, coupled with ours, would be discussed together below, in order to conveniently obtain a total understanding of their characteristics.

The SiO_2, Al_2O_3, and MgO contents of these meta-pelites vary between 63.71% and 74.61%, 14.20% and 17.31%, 0.56% and 1.95%, respectively. There is no correlation between SiO_2 and Al_2O_3, indicating that the feasible mineralogical control on major and trace elements cannot be evaluated based on a single population. Al and Ti are both immobile in nature, thus they are tending to be enriched in residual sediments with different Al/Ti ratios (Young and Nesbitt, 1998). The strongly positive correlation between Al_2O_3 and TiO_2 infers a highly weathered condition of provenance and the average Al_2O_3 content (15.89 wt.%) is slightly greater than those of Archean and post-Archean crust (15 wt.%) (Rudnick and Fountain, 1995), suggesting that average source material was subject to excessive weathering. In addition, the samples have lower SiO_2/Al_2O_3 (<5) and K_2O/Na_2O ratios (<1.5), not reflecting secondary silicification and K-metasomatism.

Key trace element abundances in the meta-pelites are Zr (142.11–300 ppm), Hf (3.5–5.94 ppm), Rb (55.47–99.50 ppm), Ba

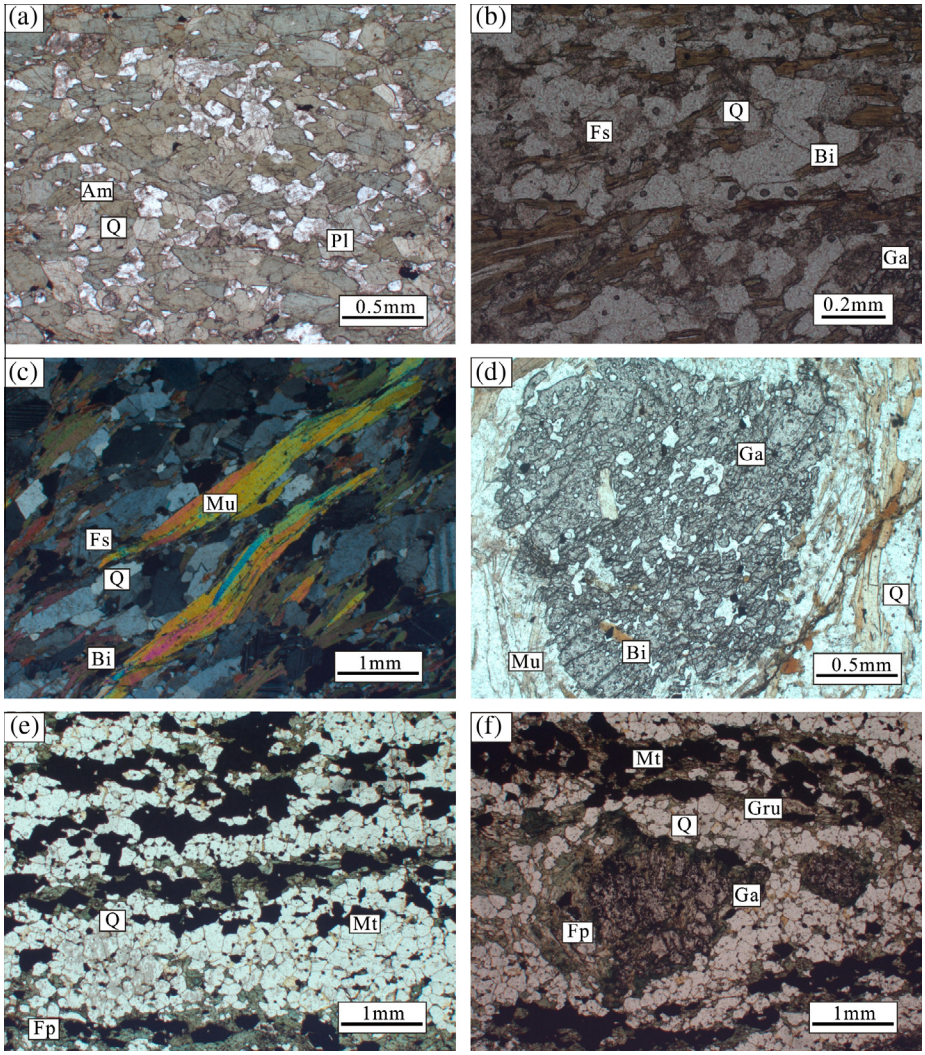

Fig. 4. Micro-photographs of the Wangjiazhuang BIF and associated lithologies showing the mineralogy and typical textures. (a) Amphibolites composed of anhedral to subhedral amphibole (Am), unaltered plagioclase (Pl) and minor quartz (Q) (plain-polarized light). (b) Biotite leptynite comprising angular to sub-angular quartz, fresh feldspar (Fs), tabular biotite (Bi) and minor garnet (Ga), showing weakly developed foliation defined by biotite (plain-polarized light). (c) Mica schist comprising quartz, feldspar, biotite, muscovite (Mu) (between crossed polarizers). Flexural mica shows a preferred crystallographic orientation. (d) Diablastic garnet in mica schist containing quartz, biotite and opaque mineral inclusions (plain-polarized light). (e) BIF consisting mainly of alternating Fe-oxide (magnetite) (Mt) and quartz bands. Not magnetite closely associated with ferro-pargasite (FP) (plain-polarized light). (f) Scattered garnet grains with some magnetite inclusions, replaced by surrounding ferro-pargasite (plain-polarized light). Not grunerite (Gru) closely intergrown with magnetite.

(340–717.7 ppm). Average Nb/Ta (13.8) and Zr/Hf (37.27) ratios are similar to those for Archean continental crust (ACC) (12 and 40) (Rudnick and Fountain, 1995), suggesting that secondary fractionation processes are negligible (Bau, 1996). Thus, HFSE systematics can be a powerful tool for distinguishing metasomatically modified trace element compositions from sedimentary compositions (Bolhar et al., 2005).

Chondrite-normalized REE patterns are shown in Fig. 5a. All samples show variable enrichment of the light rare earth elements (LREEs) relative to the middle and heavy REE (La/Sm_N = 2.29–7.01 and La/Yb_N = 3.52–57.16). Gd/Yb_N ratios (1.27–5.07) are also quite variable, indicating significant HREE depletion. Samples also exhibit negative to negligible Eu anomalies (0.69–0.96).

4.2. Nd isotopes

Sm–Nd isotopes and concentrations of these elements for the Wangjiazhuang bulk-BIF samples and associated supracrustal rocks are presented in Table 2. One of amphibolite samples (meta-basalts) (WJZ2-2) displays a high positive $\varepsilon_{Nd}(0)$ (+19.1) and a low T_{DM} age (2.24 Ga). There is no reasonable explanation for this, therefore, the Sm–Nd isotope data of this sample is excluded from the discussion below.

Neodymium and Sm concentrations in the Wangjiazhuang BIF samples range from 3.307 to 5.196 ppm (average of 4.461 ppm) and from 0.750 to 1.182 ppm (average of 0.955 ppm), respectively. $^{143}Nd/^{144}Nd$ ratios are relatively uniform defining an average subchondritic value of ~0.511710. The Nd model ages (T_{DM}) range from 2.73 to 4.01 Ga (average of 3.16 Ga). There is some variation in ε_{Nd} (t = 2540 Ma) values (from −2.58 to +2.22) (Table 2).

The Sm–Nd isotope data of volcanic rocks from the Wutai Group, including 27 samples from Wang (2009) and 6 samples from our study, are clearly different from the Wangjiazhuang BIF in that the initial ε_{Nd} values recalculated using ~2540 Ma are consistently positive varying from 0 to +3.9 (Fig. 6). This indicates a depleted mantle source for formation of these volcanic rocks. In addition, all Sm–Nd isotope data of volcanic rocks plot along a correlation line in a conventional isochron diagram (Fig. 7) with an apparent age of 2624 ± 87 Ma (MSWD = 1.9). The initial ε_{Nd} value is 0.509334 ± 0.000096. Considering that previous trace element

Table 1
Major and trace element compositions of meta-pelites from the Wangjiazhuang BIF.

Sample	WJZ5-1[a]	WJZ5-2[a]	WJZ5-3[a]	WJZ5-4[b]	WJZ5-5[b]	WJZ5-6	WJZ5-7	WJZ5-8
wt.%								
SiO_2	74.61	63.71	67.13	66.29	66.96	69.32	68.54	70.16
TiO_2	0.19	0.70	0.48	0.27	0.82	0.36	0.75	0.41
Al_2O_3	14.20	17.07	16.46	14.57	17.31	14.83	17.10	15.57
MnO	0.05	0.07	0.02	0.08	0.13	0.04	0.06	0.07
MgO	0.56	1.95	1.66	1.80	0.71	1.02	0.86	1.36
CaO	2.07	2.66	1.95	2.62	2.66	1.97	2.02	2.39
Na_2O	2.61	3.29	2.37	2.47	5.49	2.52	3.67	4.12
K_2O	2.04	2.75	3.21	1.89	2.52	1.95	2.23	2.69
P_2O_5	0.07	0.15	0.08	0.08	0.03	0.09	0.12	0.10
TFe_2O_3	2.39	6.42	4.35	7.40	3.14	7.20	4.25	2.23
LOI	1.26	1.16	2.60	1.72	0.34	1.05	0.85	1.29
Sum	100.05	99.93	100.31	99.19	100.11	100.35	100.45	100.39
ppm								
Li	10.04	30.82	25.78	27.10	20.70	20.56	15.67	23.36
Be	2.31	1.22	1.57	1.70	2.30	1.34	2.21	1.47
Sc	3.94	14.15	8.58			10.86	7.52	5.12
V	22.24	113.84	74.00	18.90	44.30	35.23	40.63	67.89
Cr	349.70	322.42	243.50	10.10	18.70	11.20	17.52	19.25
Co	6.72	21.59	13.74	9.80	6.60	10.23	16.49	15.38
Ni	19.44	61.72	35.45	10.00	11.10	12.32	9.89	13.46
Cu	12.25	31.40	15.45	32.20	51.90	12.24	20.13	22.33
Zn	24.18	78.50	72.31	66.50	60.70	25.36	46.62	72.35
Ga	18.73	21.83	21.37			19.16	20.02	21.26
Rb	65.69	64.76	55.47	99.50	72.30	58.92	64.39	58.37
Sr	198.68	211.67	203.22	167.00	320.00	254.65	202.98	206.45
Y	13.16	12.92	10.59	37.10	4.40	11.47	10.54	13.65
Zr	142.11	149.83	209.20	144.00	300.00	167.56	183.26	148.62
Nb	15.92	7.29	10.69	12.90	6.70	8.99	10.41	13.78
Cs	2.77	6.92	3.35	9.40	1.90	4.02	5.69	7.01
Ba	689.74	479.33	717.70	340.00	603.00	503.49	603.27	654.69
La	21.92	21.10	25.24	22.60	25.50	21.21	23.42	25.78
Ce	50.70	42.43	50.01	78.20	48.20	50.82	44.56	50.54
Pr	4.25	5.37	6.30	6.80	5.07	4.30	5.42	6.50
Nd	14.00	20.05	23.93	27.00	16.50	16.32	20.01	25.12
Sm	2.40	4.02	4.17	6.36	2.35	3.20	4.12	4.06
Eu	0.66	1.07	1.03	1.52	0.69	0.89	1.12	1.26
Gd	2.01	3.35	3.43	7.04	1.96	2.46	3.57	3.56
Tb	0.32	0.49	0.48	1.12	0.18	0.32	0.52	0.62
Dy	2.02	2.61	2.50	6.86	0.84	2.34	2.78	2.34
Ho	0.42	0.49	0.47	1.50	0.14	0.50	0.54	0.57
Er	1.26	1.32	1.24	4.64	0.37	1.27	1.36	1.42
Tm	0.20	0.19	0.18	0.68	0.05	0.21	0.19	0.18
Yb	1.44	1.25	1.23	4.60	0.32	1.54	1.33	1.43
Lu	0.22	0.19	0.20	0.69	0.03	0.24	0.21	0.33
Hf	4.13	4.22	5.94	3.50	5.90	4.34	5.62	4.98
Ta	2.55	0.54	0.86	0.80	0.50	0.49	0.78	0.81
Tl	0.26	0.41	0.43			0.33	0.42	0.39
Pb	14.89	9.52	7.78	10.00	12.10	6.99	7.65	8.29
Bi	0.81	0.26	0.23	0.10	0.10	0.35	0.33	0.44
Th	24.06	6.19	10.38	4.90	8.90	7.12	6.35	7.96
U	3.47	1.41	2.41	1.30	1.80	1.78	2.35	1.69
K_2O/Na_2O	0.78	0.84	1.35	0.77	0.46	0.77	0.61	0.65
SiO_2/Al_2O_3	5.25	3.73	4.08	4.55	3.87	4.67	4.01	4.51
Nb/Ta	6.24	13.50	12.43	16.13	13.40	18.35	13.35	17.01
Zr/Hf	34.41	35.50	35.22	41.14	50.85	38.61	32.61	29.84
La/Yb_N	9.88	12.63	12.93	10.92	12.11	14.72	3.52	57.16
Gd/Yb_N	1.32	2.22	2.06	1.15	2.22	2.31	1.27	5.07
Eu/Eu^*	0.93	0.87	0.99	0.89	0.87	0.81	0.69	0.96
CIA	58.01	56.32	60.09	57.23	51.03	60.09	58.49	52.57
CIW	68.57	67.03	69.04	70.44	59.53	70.31	66.91	61.62

[a] Data from Wang et al. (2014).
[b] Data from Zhang et al. (2010).

geochemistry of these volcanic rocks likely reflect an interaction between depleted mantle-derive (MORB-like) and subduction zone-derived melts or fluids (Wang et al., 2004), the correlation line represents a mixing line. Data of the BIF and associated sedimentary rocks also scatter along the correlation line. The meta-pelites (mica schist) are all characterized by positive ε_{Nd} values and display very similar T_{DM} ages of 2.78, 2.76 and 2.75 Ga, respectively.

5. Discussion

5.1. Nature of the detrital aluminosilicate source

Wang et al. (2014) compared the PAAS-normalized REY patterns of the six Wangjiazhuang BIF samples to that of modern seawater, present-day low-temperature and high-temperature hydrothermal fluids, and other typical iron formations, and

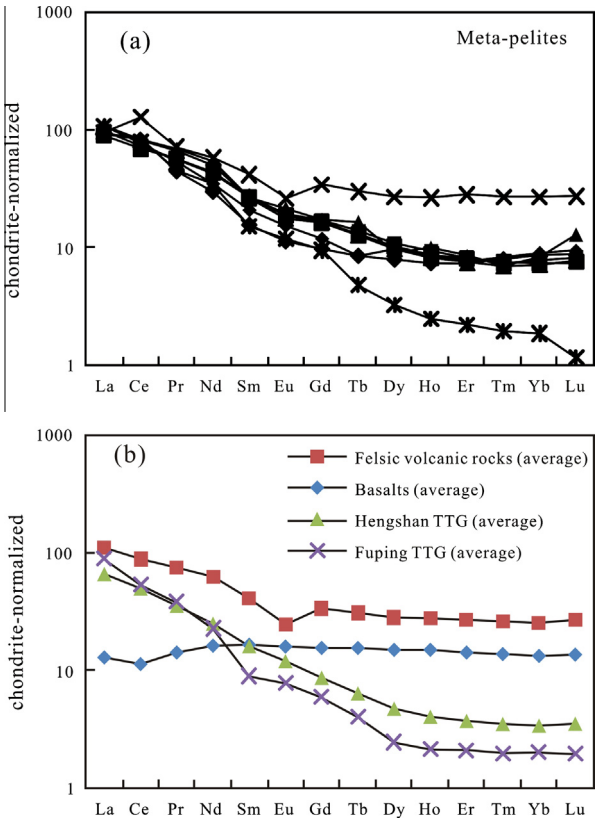

Fig. 5. Chondrite-normalized diagrams showing REE patterns of (a) meta-pelites (for data sources see Table 1) and (b) average basalts and felsic volcanics from the WGB, and Hengshan and Fuping TTG gneisses (data sources from Liu et al. (2004), Wang et al. (2004), Zhao (2012) and Wang et al. (2014)). Normalizing values after Sun and McDonough (1989).

argued that the Wangjiazhuang BIF displays clear seawater-like REY patterns strongly influenced by very limited (<1%) high-T hydrothermal fluids. In addition, the Wangjiazhuang BIF samples have higher REY abundances and lower Y/Ho ratios than those of other typical BIFs such as the Isua BIF (Bolhar et al., 2004), which are attributed to different degrees of terrigenous contamination in the BIF. This significant terrigenous input is also reflected by high and variable concentrations of Al_2O_3 (>0.5%) (Table 2) and high modal contents of garnet and ferro-pargasite in the BIF (Fig. 4e–f). From above it can be concluded that three decoupled sources control the REE compositions of the BIF: high-T hydrothermal fluids, seawater and terrigenous input. To discriminate the source of contaminants, immobile element pairs can be used (McLennan et al., 1993). It is generally accepted that Al and Ti do not fractionate during weathering, transportation and deposition (Sugitani et al., 1996). The average Al_2O_3/TiO_2 ratio for the BIF is 27.79, which is much higher than that of meta-basalts (average of 13.6) but lower than those of meta-felsic volcanic rocks (average of 45.5) and meta-pelites (average of 38.81) (Table 2). In addition, the Sm–Nd isotopic data of the BIF samples plot close to that of felsic volcanic and sedimentary rocks, except for four samples (from WJZ1-5 to WJZ1-8) with lower Al_2O_3 contents (<1%) (Fig. 7). These features collectively suggest that the aluminosilicate fraction in the iron formation was mainly derived from a source similar to that of associated clastic sediments (likely derived from pre-existing salic basement).

Terrigenous input represents a significant source of dissolved Fe(II) as a fraction of the total Fe of the Wangjiazhuang BIF. Clastic metasediments (meta-pelites) associated with the meta-basalts and BIF are regarded as products of sedimentary detritus, and thus can be used to well constrain the provenance of syn-depositional detrital contaminants.

Table 2
Sm–Nd isotopic data and selected major elements of the Wangjiazhuang BIF and associated lithologies.

Sample	Sm (ppm)	Nd (ppm)	$^{147}Sm/^{144}Nd$	$^{143}Nd/^{144}Nd$	$\pm 2\sigma_m$	$\varepsilon_{Nd}(0)$	$\varepsilon_{Nd}(t)$ (t = 2.54 Ga)	$f_{Sm/Nd}$	T_{DM}	Al_2O_3[a] (wt.%)	TiO_2[a] (wt.%)	TFe_2O_3[a] (wt.%)	SiO_2[a] (wt.%)
BIF													
WJZ1-1	0.799	4.472	0.1390	0.511737	0.000013	−17.6	1.27	−0.29	2.87	1.20	0.04	47.99	43.67
WJZ1-2	1.182	5.101	0.1400	0.511802	0.000013	−16.3	2.22	−0.29	2.78	4.78	0.16	31.67	55.19
WJZ1-3	0.750	4.51	0.1085	0.511196	0.000012	−28.1	0.71	−0.45	2.82	1.00	0.06	44.65	44.93
WJZ1-4	0.927	5.196	0.1078	0.511241	0.000011	−27.3	1.82	−0.45	2.73	2.44	0.07	35.50	54.79
WJZ1-5	1.071	4.752	0.1362	0.511557	0.000010	−21.1	−1.31	−0.31	3.12	0.87	0.04	47.82	46.11
WJZ1-6	0.967	3.307	0.1768	0.512173	0.000008	−9.1	−2.58	−0.10	4.01	0.62	0.02	49.43	45.70
WJZ1-6r[b]	0.960	3.320	0.1761	0.512140	0.000010	−9.7	−3.00	−0.10	4.07				
WJZ1-7	1.113	4.838	0.1592	0.511962	0.000009	−13.2	−0.94	−0.19	3.31	0.89	0.03	47.20	46.42
WJZ1-8	0.834	3.562	0.1658	0.512014	0.000010	−12.2	−2.09	−0.16	3.60	0.57	0.02	50.30	47.17
Assoc. rocks													
WJZ2-2/ Amphibolite	2.672	6.594	0.2453	0.513618	0.000012	19.1	3.25	0.25	2.24	13.21	1.33	14.66	52.83
WJZ2-3	1.432	4.308	0.2012	0.512911	0.000011	5.3	3.87	0.02	2.94	14.39	0.65	11.82	48.45
WJZ2-4	2.675	7.745	0.2091	0.513044	0.000011	7.9	3.89	0.06	3.60	13.66	1.19	15.24	50.07
WJZ2-5	2.914	8.498	0.2076	0.512985	0.000011	6.8	3.23	0.06	4.16	13.97	1.27	15.62	49.94
WJZ3-1/ Hornblende leptynite	3.399	19.26	0.1069	0.511185	0.000011	−28.4	1.01	−0.46	2.80	14.46	0.50	6.46	66.62
WJZ4-1/Biotite leptynite	8.993	38.33	0.1420	0.511901	0.000011	−14.4	3.52	−0.28	2.65	12.51	0.26	7.98	69.90
WJZ4-2	9.706	41.77	0.1407	0.511858	0.000009	−15.2	3.11	−0.28	2.69	12.48	0.21	6.53	69.86
WJZ5-1/Mica schist	2.756	16.70	0.0999	0.511072	0.000010	−30.5	1.09	−0.49	2.78	14.20	0.19	2.39	74.61
WJZ5-2	4.234	21.76	0.1178	0.511404	0.000009	−24.1	1.73	−0.40	2.76	17.07	0.70	6.42	63.71
WJZ5-3	4.415	25.19	0.1061	0.511202	0.000011	−28.0	1.59	−0.46	2.75	16.46	0.48	4.35	67.13
BCR-2[c]	6.746	29.831	0.1367	0.512646	0.000011								

[a] Major oxides contents from Wang et al. (2014) except for WJZ1-7 and WJZ1-8; total Fe reported as Fe_2O_3.
[b] *r* in sample name denotes a replicate digestion and analysis of the same sample.
[c] Average of 2 separate digestions of BCR-2 Columbia River basalt reference material (United States Geologic Survey).

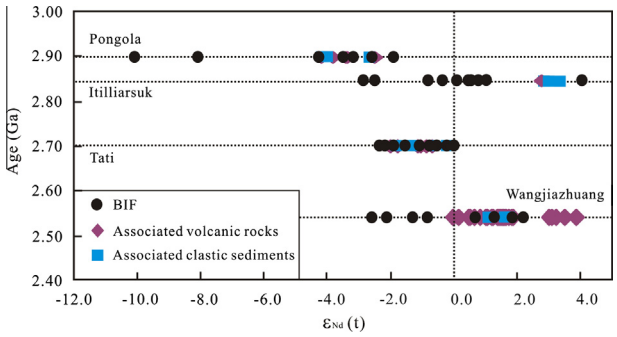

Fig. 6. Initial $\varepsilon_{Nd}(t)$ values between the Wangjiazhuang BIF and other Archean BIFs including the 2.9 Ga Pongola BIF (Alexander et al., 2008), the 2.7 Ga Tati BIF (Døssing et al., 2009), the 2.9 Ga Itilliarsuk BIF (Haugaard et al., 2013). Data of associated volcanic rocks and clastic sediments are also included for comparison (Wang, 2009; Mukasa et al., 2013).

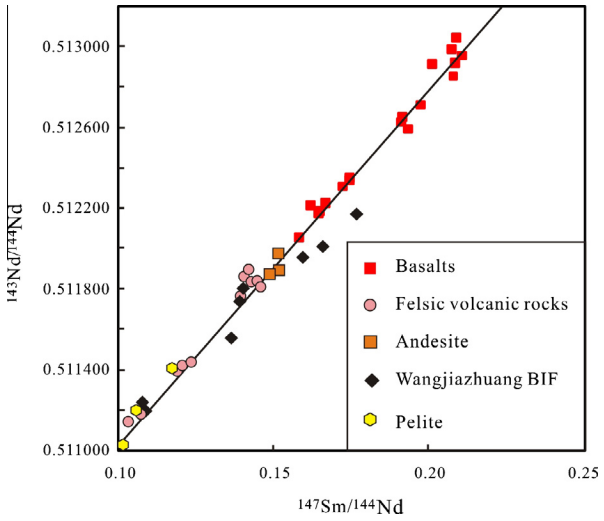

Fig. 7. Sm–Nd isochron diagram with data from the Wangjiazhuang BIF and associated rocks in the WGB. Data are from Wang (2009) and this study.

5.1.1. Provenance of meta-pelites

Intense metamorphism and deformation renders conclusive identification of the origin for these sediments problematic without reliance on geochemical fingerprints. Clastic sedimentary rocks with various geochemical features can be produced by mixing of different source rocks (Arndt and Goldstein, 1987). REE patterns are generally accepted as among the most reliable indicators of sediment provenance (Taylor and McLennan, 1985). Chondrite-normalized REE patterns of meta-pelites and potential source lithologies from the Wutai greenstone belt are shown in Fig. 5. All the meta-pelite samples are characterized by moderately to highly fractioned REE patterns with the La/Yb_N rations varying from 3.52 to 57.16. The presence of slight negative Eu anomalies ($Eu/Eu^* = 0.69–0.99$) (Table 1) for these samples indicates that intracrustal igneous processes such as partial melting or fractional crystallization of plagioclase probably did not affect the provenance rocks to a large degree (McLennan et al., 1995). Most of the volcanic sequences in this area are of bimodal character with LREE-depleted mafic volcanics and relatively LREE-enriched felsic volcanics; plutonic rocks are mostly LREE enriched and a wide range in composition (Wang et al., 2004; Liu et al., 2004; Zhao, 2012). Thus, we conclude that the meta-pelite samples are derived predominantly from a felsic source.

Moreover, incompatible to compatible element ratios, such as La/Sc and Th/Sc, have been proven to be useful tools for discriminating felsic and mafic materials (Taylor and McLennan, 1985; Cullers and Podkovyrov, 2000). In the La–Th–Sc ternary diagram (Fig. 8), all samples except one cluster in compositions of meta-felsic volcanic rocks from the WGB and plot away from the meta-basalt end member. In addition, on the plot of La/Th vs. Hf (Fig. 9a), most data show a mixing trend between felsic and recycled old sedimentary sources, mainly indicative of felsic sources.

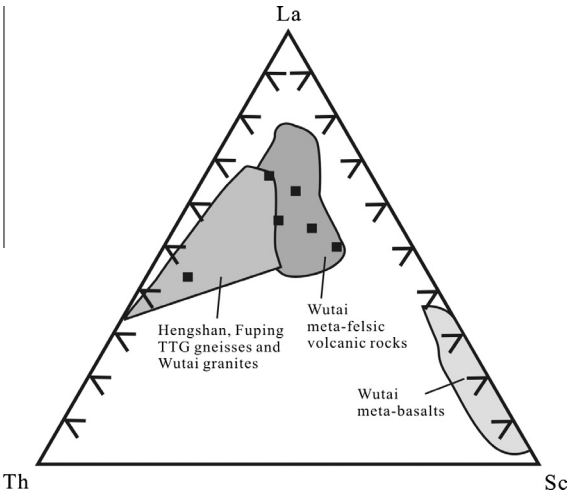

Fig. 8. Plot of the meta-pelite samples in a La–Th–Sc ternary diagram. Data sources: Hengshan TTG gneisses (Zhao, 2012), Fuping TTG gneisses and Wutai granitoids (Liu et al., 2004), meta-basalts and meta-felsic volcanic rocks from the WGB (Wang et al., 2004, 2014).

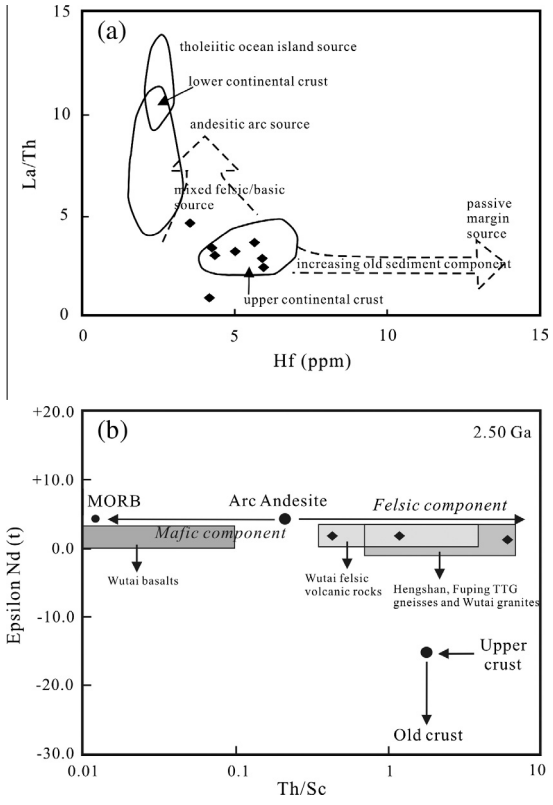

Fig. 9. (a) Source rock discrimination diagrams for the meta-pelite samples on La/Th vs. Hf (modified after Floyd and Leveridge, 1987). Average reference compositions are from Condie (1993). (b) $\varepsilon_{Nd}(2.5\ Ga)$ vs. Th/Sc diagrams of the meta-pelite samples. End members compositions are from McLennan et al. (1993). Data sources are same to Fig. 8.

These above imply again that felsic rocks were an important component to the provenance.

Radiogenic isotopes in combination with geochemical data can be instrumental in understanding the nature of sediment sources (McLennan et al., 1990; Tran et al., 2003). It was suggested that sedimentary rocks with relatively low Th/Sc ratios and high $\varepsilon_{Nd}(t)$ values are likely to be derived from less differentiated, young source terranes, whereas high Th/Sc ratios and low $\varepsilon_{Nd}(t)$ values probably imply an upper crustal source (McLennan et al., 1990, 1993; Wang et al., 2012). Fig. 9b plots ε_{Nd} (calculated at the time of sedimentation, 2.5 Ga) values against Th/Sc ratios. Shown for reference is the location of typical upper crust, intermediate island arc compositions, and MORB at 2.5 Ga. Samples of meta-felsic volcanic rocks and granites in the WGB and the Hengshan and Fuping TTGs are also plotted. All the meta-pelite samples scatter between the late Archean felsic-volcanics and TTG gneisses and granitoids fields, indicating that felsic igneous rocks from the older or coeval less differentiated terrane contributed the major source. Zhao et al. (2010) argued that the Wutai granitoids cannot be generated directly from a mantle source but must have been derived by partial melting of juvenile crust, which provide another support for the existence of less differentiated terrane.

In summary, the meta-pelites appear to be derived entirely from fairly well mixed contemporaneous or aged felsic igneous rocks, similar in composition to felsic volcanic rocks presently exposed in the WGB region. The ε_{Nd} at the time of sedimentation (+1.1 to +1.7) values are much lower than the average mantle at that time (ε_{Nd} = +4.5), which may simply reflect the less depleted mantle sources of the volcanic arcs (McLennan et al., 1993). Work is in progress to ascertain whether these sources are penecontemporaneous with the metasediments or whether they also contain an older component.

5.1.2. Source weathering

Weathering in source areas can cause relative depletion of alkali and alkaline earth elements and corresponding enrichment of Al_2O_3 (and TiO_2) in terrigenous sedimentary rocks (Bolhar et al., 2005). The extent of source area weathering can be quantified with the Chemical Index of Alteration (CIA: Nesbitt and Young, 1989) or the Chemical Index of Weathering (CIW: Harnois, 1988). Unweathered basalts and granitoids are characterized by CIA values of 30–45 and 45–55, respectively, while average shales have CIA values of 45 (ACC) to 70 (PAAS) (Fig. 10). The meta-pelites have CIA values of 51–60, which are less than for PAAS. Moreover, the meta-pelite samples have mean CIW values of 67 (60–70), which are also lower than those of PAAS (83). These suggest a relatively modest weathering history affecting the source of these samples as indicated by the very small variations of K_2O/Na_2O (0.5–1.4). However, the strong linear correlation between Al_2O_3 and TiO_2 (R^2 = 0.94) suggests severe weathering in the source rocks (Young and Nesbitt, 1998).

Data are plotted on a ternary diagram of molecular proportions A (Al_2O_3)–CN ($CaO^* + Na_2O$)–K(K_2O), where CaO^* is the CaO in the silicate fraction only (Fig. 10). Plotted for reference are several idealized mineral compositions (Nesbitt and Young, 1984). The meta-pelite samples define a trend parallel to the A–CN join and extend towards the A apex, essentially similar to the trends for surface weathering of felsic rocks. Interestingly, meta-pelites reflecting the lowest degrees of source weathering have major element compositions comparable to average TTG and felsic volcanic rocks. This is in line with above trace element systematics, indicating that the latter lithologies qualify as potential source components. No apparent enrichments in K are also observed to rule out the possibility of the secondary addition of K^+.

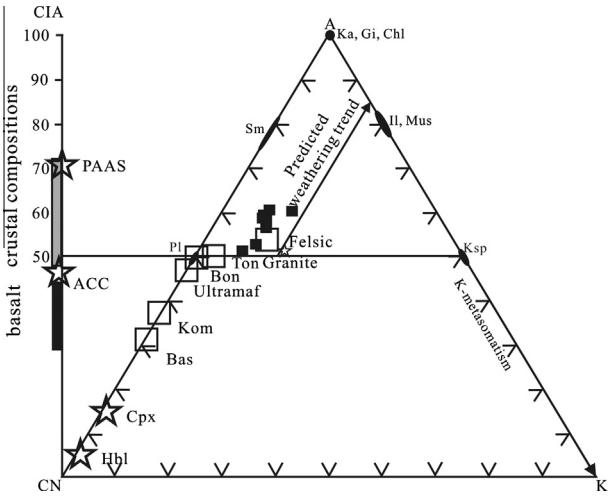

Fig. 10. Ternary plot of molecular proportions Al_2O_3(A)–CaO^*+Na_2O(CN)–K_2O(K) for the meta-pelite samples associated with the Wangjiazhuang BIF (after Nesbitt and Young, 1989) (for data sources see Table 1). Also shown are idealized mineral and igneous rocks compositions: Ka = kaolinite, Gi = gibbsite, Chl = chlorite, Il = illite, Mus = muscovite, Ksp = K-feldspar, Sm = smectite, Pl = plagioclase, Cpx = clinopyroxene, Hbl = Hornblende, Bas = basalt, Kom = Komatiite, Ultramafic = unltramafic rock, Bon = boninite, Ton = tonalite, Felsic = felsic volcanic rocks (Wang et al., 2004).

5.2. Inferences for sources of the BIF

It is necessary to examine the possibility that primary Nd isotopic signals recorded in BIFs may be disturbed by post-depositional processes. The Na- and Fe-bearing amphibole riebeckite was found to accompany disturbed Sm–Nd isotopic compositions in the Hamersley IFs (Alibert and McCulloch, 1993). However, the Wangjiazhuang BIF samples display very low Na content (<0.5%) (Wang et al., 2014), indicating the absence of only minor amounts of riebeckite. Generally speaking, the Sm–Nd isotopic system is resistant to metamorphism. And for the BIFs that have experienced a wide range of metamorphic overprint, consistent Nd isotopic results are obtained (Shimizu et al., 1990; Bau et al., 1997; Alexander et al., 2009). Bau et al. (1997) reported Sm–Nd data for the Kuruman and Penge BIFs of the Transvaal Supergroup in South Africa, which are stratigraphically equivalent. Although different degrees of metamorphism covering the Kuruman (<200 °C) and Penge (>500 °C) BIFs, both BIFs yield very similar Sm–Nd isotopic ratios and REE patterns.

The Wangjiazhuang BIF samples contain high Al_2O_3 content (>0.5%), which renders them unsuitable as proxies for the marine water that precipitated them. But these samples do provide Nd isotopic information regarding the material source of the BIF. ε_{Nd}(2.54 Ga) of the BIF samples varies as a function of Al content (Fig. 11a), with samples containing more than 1% Al_2O_3 displaying relatively uniform positive ε_{Nd}(2.54 Ga) between +0.71 and +2.22. Samples containing less than 1% Al_2O_3 are significantly less radiogenic, displaying negative ε_{Nd}(2.54 Ga) between −0.94 and −2.58. The difference between these two groups of ε_{Nd}(2.54 Ga) values exceeds the analytical error of the measurements. The positive correlation between Al_2O_3 and $\varepsilon_{Nd}(t)$ suggests that the aluminum content is derived by sources with positive $\varepsilon_{Nd}(t)$ of approximately +1.5, similar to those of the above meta-pelites, and seawater responsible for deposition of the BIF was less radiogenic with ε_{Nd}(2.54 Ga) values similar to or less than −2.6. This relationship also reveals the detrital component was well-mixed and that the sediment source did not change dramatically during the time of BIF deposition. However, this relationship is in direct contrast to the ~2.95 Ga BIF from the Pietersburg greenstone belt in the South Africa (Alexander et al., 2009). They argued that negative $\varepsilon_{Nd}(t)$

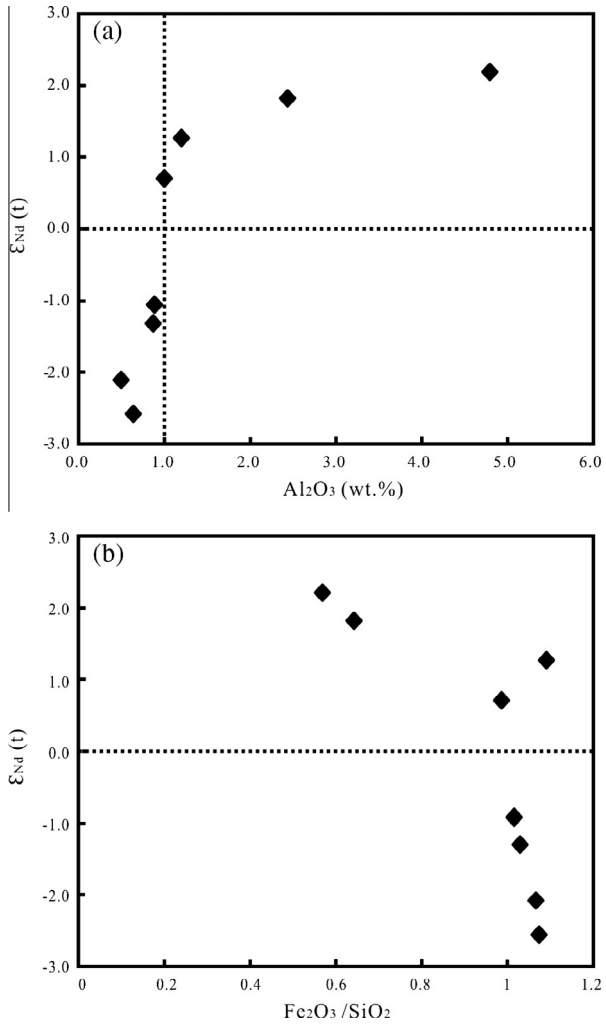

Fig. 11. The relationship between (a) the initial ε_{Nd} and Al and (b) the initial ε_{Nd} and Fe_2O_3/SiO_2 ratios for the Wangjiazhuang bulk-BIF samples (for data sources see Table 2).

values are sourced from nearby old enriched continental crust, which thus resulted in a negative Al–$\varepsilon_{Nd}(t)$ relationship. Taking these into consideration, nature of the Al-rich detritus in BIFs was of significance for producing various Al–$\varepsilon_{Nd}(t)$ relationships.

A two-component mixing between a detrital source and the pure seawater might adequately model the Nd isotopic data. However, considering that pure BIFs are best described already as mixtures of two-components based on characteristics of their major and trace elements: high-T hydrothermal fluids and ambient seawater (Wang et al., 2014), this simple mixing actually reflects three end members.

The Fe_2O_3/SiO_2–$\varepsilon_{Nd}(t)$ relationship is shown in Fig. 11b. Previous studies have shown that the Fe component of BIFs has a depleted Nd isotopic signature suggesting that mid-ocean ridges and/or hotspot activity were the major source of iron (e.g., Holland, 1973; Morris and Horowitz, 1983; Jacobsen and Pimentel-Klose, 1988; Bau et al., 1997; Frei and Polat, 2007). For example, for the 3.7 Ga Isua BIF, Frei and Polat (2007) reported a positive relationship between the $\varepsilon_{Nd}(t)$ and iron content. They argued that there are two distinct REE sources, one being seafloor-vented hydrothermal fluids (iron-rich) ($\varepsilon_{Nd}(t) = +3.1$), the other being ambient seawater (iron-poor) ($\varepsilon_{Nd}(t) = +1.6$). However, this is not the case for the Wangjiazhuang BIF. There is no obvious correlation between Fe_2O_3/SiO_2 ratios and $\varepsilon_{Nd}(t)$. Close examination of the samples containing Al_2O_3 less than 1% suggests that the Fe-rich source is associated with a more enriched source ($\varepsilon_{Nd}(t) = -2.58$). Nevertheless, before attempting to constrain the source of iron using Nd isotopic information, a significant premise should be taken into account that the Fe/Nd ratios did not change significantly in the ancient ocean. Some processes controlling the different geochemical behaviors of Fe and Nd in the Archean ocean have been recently discussed by Alexander et al. (2008), for example, pyrite precipitation close to hydrothermal vent sites fractionated Fe and Nd. Thus, definite statements are not allowed to be made regarding the Fe source to BIFs based upon Nd isotope systematics.

Regardless of the Fe source to BIFs, the use of Sm–Nd isotopes for discerning the relative impact of hydrothermal vs. continentally derived REE fluxes should be possible. The above interpretation of Sm–Nd characteristics implies that for the pure BIF samples the material source is associated with a low Sm/Nd source and at the same time with a source that is significantly enriched ($\varepsilon_{Nd}(t) \approx -2.6$). Three explanations for the unusual relationship can be put forward:

(1) The source reservoir is the subaerial weathering of an enriched continental crust exposed in the hinterland. Within the framework of this model, the continental-type Nd was thought to represent the riverine/aeolian input. But it is not known whether these continent-derived REE were transported into seawater in dissolved form (as "free" REE^{3+} ions and dissolved REE(III) complexes or in solid form (incorporated into minerals or absorbed onto particle surfaces) (Bau et al., 1997). Clastic metasediments (meta-pelites) associated with the volcanics and BIF in the WGB indicate only incipient source weathering, and show geochemical features similar to felsic rocks. They are sedimentary erosion products of detrital components from a chemically evolved landmass consisting mainly of felsic igneous rocks. It appears likely that ambient seawaters (at least in the depositional basin of the WGB) could have been chemically dominated by continental riverine input from weathering of this depleted landmass. This is compatible with positive Al–$\varepsilon_{Nd}(t)$ relationships for the BIF samples (Fig. 11a). Thus, for the relatively pure BIF samples, the traditionally inferred high-T hydrothermal fluids could be responsible.

However, the ~2.9 Ga Pongola iron formation in South Africa records consistently negative $\varepsilon_{Nd}(t)$ values (Alexander et al., 2008) (Fig. 6). By obtaining equivalent negative $\varepsilon_{Nd}(t)$ values for interbedded shales and different REE+Y patterns with distinctly MREE-enriched humps for the BIF samples, they argued against mid-ocean hydrothermal systems as the dominant REY sources but instead proposed that the REY content in the BIF was primarily derived from weathering of the adjacent enriched continental crust. Moreover, in this particular case, these REY contents are not coupled with Al-rich detritus as indicated by compositions of the BIF. But recently, Mukasa et al. (2013) carried out a detailed geochronological and geochemical research on the volcanic sequence of the Pongola Supergroup. Although trace element distributions for these volcanics show characteristics similar to those of modern arcs, including negative anomalies in Th, Ta, Nb, Ce and P, they argued that these features may have been inherited from previously formed crust. Based on evidence of rapid deposition, a preponderance of intermediate lavas, discordance of bounding crustal blocks and consistent structural trends in this area, they proposed a continental arc basin setting rather than a passive continental margin for formation of the Pongola Supergroup. Interestingly, $\varepsilon_{Nd}(t)$ values of volcanics range from −2.55 to −4.20 (Fig. 6), showing a striking similarity with those of above-mentioned shales and the BIF. Thus, it can be concluded that submarine

hydrothermal fluids derived from aged enriched mantle lithospheric materials, rather than weathering of the continental crust, exerted much effects on controlling the REE source of the BIF. In this regard, so far, the scenario that the solutes in ambient seawater were primarily from weathering of continental crust still remains controversial.

(2) Another possible scenario is that high-T hydrothermal fluids, as a significant component of source materials, were derived from interaction with an enriched mantle source (explaining the negative $\varepsilon_{Nd}(t)$ values) and then to different degrees mixed with ambient seawater and terrigenous contaminants that obtained their signatures through weathering of a predominantly depleted source (explaining the positive $\varepsilon_{Nd}(t)$ values). A similar conclusion has been put forward by Døssing et al. (2009) for the BIFs from the Tati greenstone belt (TGB) in the northeast of Botswana. In their study, there exists a negative correlation between Fe_2O_3 and Sm–Nd isotopes of the TGB BIFs. The iron-rich source is associated with a source that is significantly enriched ($\varepsilon_{Nd}(t) = -2.5$) relative to the Si-source ($\varepsilon_{Nd}(t) = -0.4$). Combining with negative $\varepsilon_{Nd}(t)$ values measured for associated volcanic rock (average of −1.3) and the less negative $\varepsilon_{Nd}(t)$ values defined by sedimentary rocks (average of −0.4) (Fig. 6), they proposed that mixing of two essential sources can explain the features of the TGB BIFs, namely seafloor-vented hydrothermal fluids that received their Sm–Nd isotopic signature from enriched mantle lithospheric materials, and ambient surface basin waters whose REE signature was controlled by solutes derived from weathering of nearby enriched continental landmasses. However, unlike the TGB BIFs, volcanic and sedimentary rocks associated with the Wangjiazhuang BIF in the WGB display consistently positive $\varepsilon_{Nd}(t)$ values (Fig. 6). Moreover, the Hengshan and Fuping TTG gneisses and Wutai granitoids are also characterized by positive $\varepsilon_{Nd}(t)$ values, indicating that they were originated from depleted sources (Liu et al., 2002, 2004; Zhao, 2012). There is no evidence to support that the mantle source in the Hengshan–Wutai–Fuping belt had experienced an earlier enrichment (Zhao et al., 2007; Zhao and Zhai, 2013).

(3) Another interpretation is that interaction of hydrothermal fluids with underlying older terrigenous clastic sediments or enriched continental crust generated aqueous fluids with continent-type Nd isotopic composition. Interestingly, this idea is similar to the conclusion of Holland (1984), who suggested that iron in the BIFs was remobilized from terrigenous sediments. It appears that the high-T hydrothermal input indicated by positive Eu anomalies in the BIF did not overwhelm the terrestrial flux in terms of the Nd isotope signature. Similar examples of the lack of correlation between mantle-like Nd isotopic signatures and positive Eu anomalies in high-T hydrothermal fluids have been found in modern submarine hydrothermal systems (Piepgras and Wasserburg, 1985; German et al., 1995; Klinkhammer et al., 1994). For example, Piepgras and Wasserburg (1985) reported Nd isotopic data for a hydrothermal system developed on a sediment-covered ridge in the Guaymas Basin, Gulf of California. The vented hydrothermal fluid ($T > 300$ °C) migrated through a sedimentary package several hundred meters thick. In contrast to solutions from sediment-starved ridges, which show positive Eu anomalies and positive $\varepsilon_{Nd}(t)$ values (Klinkhammer et al., 1994), this solution possesses similar Eu anomalies but displays negative $\varepsilon_{Nd}(t)$ values ($\varepsilon_{Nd}(0) = -11.4$), indicating that the Nd isotopic signatures of marine fluids are controlled by compositions of host rocks (Alexander et al., 2008).

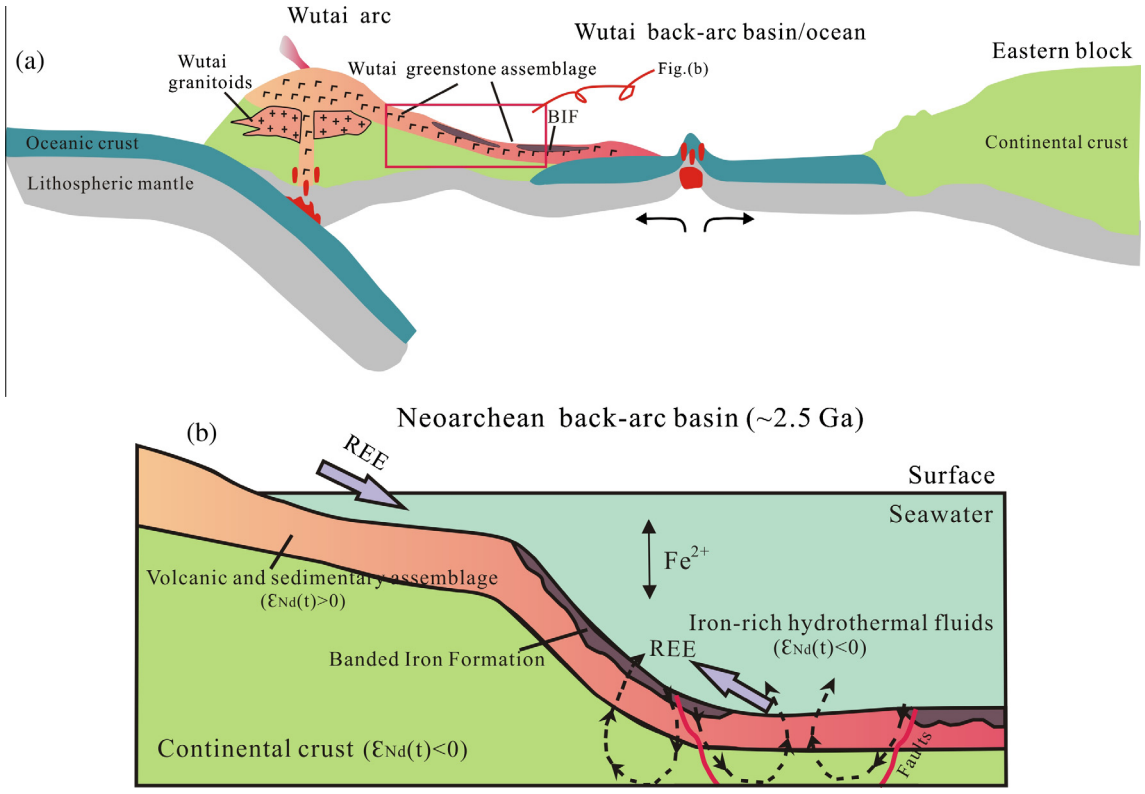

Fig. 12. Schematic diagrams showing (a) a speculative tectonic setting for the WGB (modified after Zhao et al., 2007) and (b) a sedimentary model for the Wangjiazhuang BIF in a Neoarchean back-arc basin. See text for details.

Similar explanation can be also utilized to Sm–Nd isotopic data of the 2.9 Ga Itilliarsuk BIF in the West Greenland (Haugaard et al., 2013). The Al–$\varepsilon_{Nd}(t)$ and Fe–$\varepsilon_{Nd}(t)$ relationships of the BIF samples obtained in their study show a similarity with those of the Wangjiazhuang BIF. But, especially, subchondritic $\varepsilon_{Nd}(t)$ values are found for the Fe-bands (average of −1.29) and positive $\varepsilon_{Nd}(t)$ values are observed within the silica-bands (average of +1.35). Additionally, the associated supracrustal rocks, including mta-pelites, shales, greywackes, and acidic metavolcanics, have significantly positive $\varepsilon_{Nd}(t)$ values (Fig. 6). Surprisingly, they concluded that the negative $\varepsilon_{Nd}(t)$ values found in the iron-rich layers are attributed to the submarine hydrothermal source influenced by an enriched mantle. However, it is not compatible with above positive $\varepsilon_{Nd}(t)$ values of volcanic and sedimentary rcoks. Therefore, we are more inclined to consider the interaction of submarine hydrothermal fluids with clastic sediments covering older oceanic spreading centers in terms of the inferred juvenile ocean island arc setting (Haugaard et al., 2013).

In most early models, the WGB was considered to have formed in an intra-oceanic system on the basis of geochemical features of associated volcanic rocks (Bai et al., 1992; Wang et al., 1996, 2004, 2014; Wang, 2009). However, this model is not supported by the widespread existence of remnants of 2.66–2.82 Ga older continental crust in the Wutai area (Guan et al., 2002; Zhao et al., 2002, 2007; Wilde et al., 2004). These data not only confirm the existence of ~2.7 Ga old continental crustal components in the Hengshan–Wutai–Fuping region, but also suggest that the WGB was not formed in an intra-oceanic arc but more likely to have developed on a continental margin. Based on the presence of MORB-type basalts and adakite-featured felsic volcanic rocks in the Wutai Group (Wang et al., 2004, 2014), the WGB appeared to be located in a back-arc basin and/or an inter-arc basin (Fig. 12a). At about 2540 Ma, subduction of oceanic lithosphere and further release of fluids caused partial melting in the overriding mantle wedge, leading to widespread mafic to felsic volcanism, which ultimately resulted in the formation of the WGB. At the same time, extension driven by widespread mafic to felsic volcanism led to the development of a back-arc basin or marginal sea with formation of newly formed oceanic crusts.

In conclusion, the negative $\varepsilon_{Nd}(t)$ characteristics of the Wangjiazhuang BIF were assumed to be related to the high-T hydrothermal fluids mainly derived from submarine volcanism. A possible scenario is that REE and iron (?) were obtained through long-term interaction between these fluids and the underlying old continental crust ($\varepsilon_{Nd}(t) < 0$), which then periodically mixed with ambient seawater and syn-depositional detritus that received REE through weathering of a predominantly depleted source (likely the arc) ($\varepsilon_{Nd}(t) > 0$). Taken together, these processes are ultimately responsible for the Nd isotopic features observed in the Wangjiazhuang BIF (Fig. 12b).

6. Conclusion

The 2.54 Ga Wangjiazhuang BIF, situated in the Wutai greenstone belt, is associated with lithologies including meta-basalts, meta-felsic volcanics, and meta-pelites, which have undergone amphibolite-facies metamorphism.

The associated meta-pelites are of significance for providing a good understanding of nature of terrigenous contamination in the BIF. The REE patterns of meta-pelite samples reveal that they are obviously derived from a felsic source. Moreover, trace element ratios and $\varepsilon_{Nd}(t)$ values of them further indicate that felsic igneous rocks, as primary components of the provenance, are derived from less differentiated terranes. The degree of source weathering was incipient without secondary K addition.

The Sm–Nd isotope systematics of the Wangjiazhuang BIF support mixing of REE+Y from different end members. These decoupled sources represent, respectively (1) seafloor-vented hydrothermal fluids that received their Sm–Nd isotopic signatures through interaction with the underlying old continental crust in terms of the inferred tectonic setting of the BIF, and (2) ambient basin waters and terrigenous contaminants in the BIF whose REE signatures were controlled by solutes derived from weathering of nearby landmasses (likely the arc) with a depleted feature.

Acknowledgements

This work was supported by the Major State Basic Research Programme of the People's Republic of China (No. 2012CB416601) and the National Natural Science Foundation of China (No. 41372100). Much thanks for Zhuyin Chu, Chaofeng Li and Yan Yan, they give us help in Sm–Nd analyses. We also thank Dr. Bor-ming Jahn and two anonymous reviewers for their constructive comments.

References

Alexander, B.W., Bau, M., Andersson, P., Dulski, P., 2008. Continentally-derived solutes in shallow Archean seawater: rare earth element and Nd isotope evidence in iron formation from the 2.9 Ga Pongola Supergroup, South Africa. Geochimica et Cosmochimica Acta 72, 378–394.

Alexander, B.W., Bau, M., Andersson, P., 2009. Neodymium isotopes in Archean seawater and implications for the marine Nd cycle in Earth's early oceans. Earth Planet. Sci. Lett. 283, 144–155.

Alibert, C., McCulloch, M.T., 1993. Rare earth element and Nd isotopic compositions of the banded iron-formations and associated shales from Hamersley, Western Australia. Geochim. Cosmochim. Acta 57, 187–204.

Arndt, N.T., Goldstein, S.L., 1987. Use and abuse of crust-formation ages. Geology 15, 893–895.

Bai, J., 1986. The Early Precambrian Geology of Wutaishan. Tianjin Science and Technology Press, Tianjin, China, p. 435.

Bai, J., Wang, R.Z., Guo, J.J., 1992. The major Geologic Events of Early Precambrian and Their Dating in Wutaishan Region. Geological Publishing House (in Chinese), Beijing, pp. 34–55.

Bau, M., 1996. Controls on the fractionation of isovalent trace elements in magmatic and aqueous systems: evidence from Y/Ho, Zr/Hf and lanthanide tetrad effect. Contrib. Miner. Petrol. 123, 323–333.

Bau, M., Dulski, P., 1996. Distribution of yttrium and rare-earth elements in the Penge and Kuruman iron-formations, Transvaal Supergroup, South Africa. Precambr. Res. 79, 37–55.

Bau, M., Dulski, P., 1999. Comparing yttrium and rare-earth in hydrothermal fluids from the Mid-Atlantic Ridge: implications for Y and REE behaviour during near vent mixing and for the Y/Ho ratio of Proterozoic seawater. Chem. Geol. 155, 77–90.

Bau, M., Höhndorf, A., Dulski, P., Beukes, N.J., 1997. Sources of rare-earth elements and iron in Paleoproterozoic ironformations from the Transvaal Supergroup, South Africa: evidence from neodymium isotopes. J. Geol. 105, 121–129.

Bekker, A., Slack, J.F., Planavsky, N., Krapež, B., Hofmann, A., Konhauser, K.O., Rouxel, O.J., 2010. Iron formation: the sedimentary product of a complex interplay among mantle, tectonic, oceanic, and biospheric processes. Econ. Geol. 105, 467–508.

Bolhar, R., Kamber, B.S., Moorbath, S., Fedo, C.M., Whitehouse, M.J., 2004. Characterisation of early Archaean chemical sediments by trace element signatures. Earth Planet. Sci. Lett. 222, 43–60.

Bolhar, R., Kamber, B.S., Moorbath, S., Whitehouse, M.J., Collerson, K.D., 2005. Chemical characterization of Earth's most ancient clastic metasediments from the Isua Greenstone Belt, southern West Greenland. Geochim. Cosmochim. Acta 69, 1555–1573.

Chu, Z.Y., Wu, F.Y., Walker, R.J., Rudnick, R.L., Pitcher, L., Puchtel, I.S., Yang, Y.H., Wilde, S.A., 2009. Temporal evolution of the lithospheric mantle beneath the eastern North China Craton. J. Petrol. 50, 1857–1898.

Condie, K.C., 1993. Chemical composition and evolution of the upper continental crust: contrasting results from surface samples and shales. Chem. Geol. 104, 1–37.

Cullers, R.L., Podkovyrov, V.N., 2000. Geochemistry of the Mesoproterozoic Lakhanda shales in southeastern Yakutia, Russia: implications for mineralogical and provenance control, and recycling. Precambr. Res. 104, 77–93.

Danielson, A., Möller, P., Dulski, P., 1992. The europium anomalies in banded iron formations and the thermal history of the oceanic crust. Chem. Geol. 97, 89–100.

DePaolo, D.J., 1981. Neodymium isotopes in the Colorado Front Range and crust–mantle evolution in the proterozoic. Nature 291, 193–196.

Derry, L.A., Jacobsen, S.B., 1990. The chemical evolution of Precambrian seawater: evidence from rare earth elements in banded iron formations. Geochim. Cosmochim. Acta 54, 2965–2977.

Døssing, L.N., Frei, R., Stendal, H., Mapeo, R.B.M., 2009. Characterization of enriched lithospheric mantle components in ~2.7 Ga Banded Iron Formations: an example from the Tati Greenstone Belt. Northeastern Botswana. Precambrian Res. 172, 334–356.

Floyd, P., Leveridge, B., 1987. Tectonic environment of the Devonian Gramscatho basin, south Cornwall: framework mode and geochemical evidence from turbiditic sandstones. J. Geol. Soc. 144, 531–542.

Frei, R., Polat, A., 2007. Source heterogeneity for the major components of ~3.7 Ga Banded Iron Formations (Isua Greenstone Belt, Western Greenland): tracing the nature of interacting water masses in BIF formation. Earth Planet. Sci. Lett. 253, 266–281.

German, C.R., Barreiro, B.A., Higgs, N.C., Nelson, T.A., Ludford, E.M., Palmer, M.R., 1995. Seawater-metasomatism in hydrothermal sediments (Esca-naba Trough, northeast Pacific). Chem. Geol. 119, 175–190.

Guan, H., Sun, M., Wilde, S.A., Zhou, X.H., Zhai, M.G., 2002. SHRIMP U–Pb zircon geochronology of the Fuping Complex: implications for formation and assembly of the North China Craton. Precambr. Res. 113, 1–18.

Harnois, L., 1988. The CIW index: a new chemical index of weathering. Sed. Geol. 55, 319–322.

Haugaard, R., Frei, R., Stendal, H., Konhauser, K.O., 2013. Petrology and geochemistry of the ~2.9 Ga Itilliarsuk banded iron formation and associated supracrustal rocks, West Greenland: source characteristics and depositional environment. Precambr. Res. 229, 150–176.

Holland, H.D., 1973. The oceans: a possible source of iron in iron-formations. Econ. Geol. 68, 1169–1172.

Holland, H.D., 1984. The Chemical Evolution of the Atmosphere and the Oceans. Princeton University Press, New York, p. 582.

Jacobsen, S.B., Pimentel-Klose, M.R., 1988. Nd isotopic variations in Precambrian banded iron formations. Geophys. Res. Lett. 15, 393–396.

James, H.L., 1954. Sedimentary facies of iron-formation. Econ. Geol. 49, 235–293.

Klinkhammer, G.P., Elderfield, H., Edmond, J.M., Mitra, A., 1994. Geochemical implications of rare-earth element patterns in hydrothermal fluids from mid-ocean ridges. Geochim. Cosmochim. Acta 58, 5105–5113.

Kusky, T.M., Li, J.H., 2003. Paleoproterozoic tectonic evolution of the North China Craton. J. Asian Earth Sci. 22, 383–397.

Li, Y.H., 2008. The study on geological features and genesis of iron deposit in Wangjiazhuang Region, Yuanping City, Shanxi Province. Master Thesis, China University of Geosciences (Beijing), p. 48.

Li, Z.H., Zhu, X.K., Tang, S.H., Li, J., Liu, H., 2010. Characteristics of rare earth elements and geological significations of BIFs from Jidong, Wutai and Lüliang area. Geoscience 24, 840–846.

Liu, S.W., Pan, Y.M., Li, J.H., Zhang, J., Li, Q.G., 2002. Geological and isotopic geochemical constraints on the evolution of the Fuping Complex, North China Craton. Precambr. Res. 117, 41–56.

Liu, S.W., Pan, P.M., Xie, Q.L., Zhang, J., Li, Q.G., 2004. Archean geodynamics in the Central Zone, North China Craton: constraints from geochemistry of two contrasting series of granitoids in the Fuping and Wutai Complexes. Precambr. Res. 130, 229–249.

McLennan, S.M., Taylor, S.R., McCulloch, M.T., Maynard, J.B., 1990. Geochemical and Nd–Sr isotopic composition of deep-sea turbidites: crustal evolution and plate tectonic association. Geochim. Cosmochim. Acta 54, 2015–2050.

McLennan, S.M., Hemming, S., McDaniel, D.K., Hanson, G.N., 1993. Geochemical approaches to sedimentation, provenance, and tectonics. Geol. Soc. Am. Spec. Pap. 284, 21–40.

McLennan, S.M., Hemming, S.R., Taylor, S.R., Eriksson, K.A., 1995. Early Proterozoic crustal evolution: geochemical and Nd–Pb isotopic evidence from metasedimentary rocks, southwestern North America. Geochim. Cosmochim. Acta 59, 1153–1177.

Michard, A., 1989. Rare earth element systematics in hydrothermal fluids. Geochim. Cosmochim. Acta 53, 745–750.

Morris, R.C., Horowitz, R.C., 1983. The origin of the iron-formation-rich Hamersley Group of Western Australia-deposition on a platform. Precambr. Res. 21, 273–297.

Mukasa, S.B., Wilson, A.H., Young, K.R., 2013. Geochronological constraints on the magmatic and tectonic development of the Pongola Supergroup (Central Region), South Africa. Precambr. Res. 224, 268–286.

Nesbitt, H.W., Young, G.M., 1984. Prediction of some weathering trend of plutonic and volcanic rocks based on thermodynamic and kinetic consideration. Geochim. Cosmochim. Acta 48, 1523–1534.

Nesbitt, H.W., Young, G.M., 1989. Formation and diagenesis of weathering profiles. J. Geol. 97, 129–147.

Niu, X.L., Li, J.H., 2006. Geochronology and geological event sequences of Hengshan–Wutai Precambrian complex. Acta Scientiarum Naturalium Universitatis Pekinensis 1, 1–7.

Piepgras, D.J., Wasserburg, G.J., 1985. Strontium and neodymium isotopes in hot springs on the East Pacific Rise and Guaymas Basin. Earth Planet. Sci. Lett. 72, 341–356.

Qian, J.H., Wei, C.J., Zhou, X.W., Zhang, Y.H., 2013. Metamorphic P–T paths and New Zircon U–Pb age data for garnet-mica schist from the Wutai Group, North China Craton. Precambr. Res. 233, 282–296.

Rudnick, R., Fountain, D.M., 1995. Nature and composition of the continental crust: a lower crustal perspective. Rev. Geophys. 33, 267–309.

Shimizu, H., Umemoto, N., Masuda, A., Appel, P.W.U., 1990. Sources of iron-formations in the Archean Isua and Malene supracrustals, West Greenland: evidence from La–Ce and Sm–Nd isotopic data and REE. Geochim. Cosmochim. Acta 54, 1147–1154.

Sugitani, K., Horiuchi, Y., Adachi, M., Sugisaki, R., 1996. Anomalously low Al_2O_3/TiO_2 values for Archean cherts from the Pilbara Block, Western Australia-possible evidence for extensive chemical weathering on the early earth. Precambr. Res. 80, 49–76.

Sun, S.S., McDonough, W.F., 1989. Chemical and isotopic systematics of oceanic basalts: implications for mantle composition and processes. Geol. Soc. Lond. Spec. Pub. 42, 313–345.

Taylor, S.R., McLennan, S.M., 1985. The Continental Crust: Its Composition and Evolution. Blackwell Scientific Publications, Oxford, UK, p. 312.

Tian, Y.Q., 1991. Geology and Mineralization of the Wutai–Hengshan Greenstone Belt. Shanxi Science and Technology Press, Taiyuan, China, p. 270.

Tran, H.T., Ansdell, K., Bethune, K., Watters, B., Ashton, K., 2003. Nd isotope and geochemical constraints on the depositional setting of Paleoproterozoic metasedimentary rocks along the margin of the Archean Hearne craton, Saskatchewan, Canada. Precambr. Res. 123, 1–28.

Trendall, A.F., 2002. The significance of iron-formation in the Precambrian stratigraphic record. Spec. Pub. Int. Assoc. Sedimentology 33, 33–66.

Wang, C.L., Zhang, L.C., Lan, C.Y., Dai, Y.P., 2014. Petrology and geochemistry of the Wangjiazhuang banded iron formation and associated supracrustal rocks from the Wutai Greenstone Belt in the North China Craton: implications for their origin and tectonic setting. Precambrian Res., in press.

Wang, K.Y., Li, J.L., Hao, J., Li, J.H., Zhou, S.P., 1996. The Wutaishan Mountain Belt within the Shanxi Province, Northern China: a record of Neoarchaean collision tectonics. Precambr. Res. 78, 95–103.

Wang, W., Chen, F.K., Hu, R., Chu, Y., Yang, Y.Z., 2012. Provenance and tectonic setting of Neoproterozoic sedimentary sequences in the South China Block: evidence from detrital zircon ages and Hf–Nd isotopes. Int. J. Earth Sci. 101, 1723–1744.

Wang, Z.H., 2009. Tectonic evolution of the Hengshan–Wutai–Fuping complexes and its implication for the Trans–North China Orogen. Precambr. Res. 170, 73–87.

Wang, Z.H., Wilde, S.A., Wang, K.Y., Yu, L.J., 2004. A MORB-arc basalt–adakite association in the 2.5 Ga Wutai Greenstone Belt: neoarchaean magmatism and crustal growth in the North China Craton. Precambr. Res. 131, 323–343.

Wilde, S.A., Cawood, P.A., Wang, K.Y., Nemchin, A., Zhao, G.C., 2004. Determining Precambrian crustal evolution in China: a case-study from Wutaishan, Shanxi Province, demonstrating the application of precise SHRIMP U–Pb geochronology. In: Malpas, J., Fletcher, C.J.N., Ali, J.R., and Aichison, J.C. (Eds.), Aspects of the Tectonic Evolution of China: Geological Society of London, Special Publication 226, pp. 5–26.

Wilde, S.A., Cawood, P.A., Wang, K.Y., Nemchin, A., 2005. Granitoid evolution in the late Archean Wutai Complex: North China Craton. J. Asian Earth Sci. 24, 597–613.

Young, G.M., Nesbitt, H.W., 1998. Process controlling the distribution of Ti and Al in weathering profiles, siliciclastic sediments and sedimentary rocks. J. Sediment. Res. 68, 448–455.

Zhai, M.G., Santosh, M., 2013. Metallogeny of the North China Craton: link with secular changes in the evolving Earth. Gondwana Res. 24, 275–297.

Zhang, L.C., Zhai, M.G., Wan, Y.S., Guo, J.H., Dai, Y.P., Wang, C.L., Liu, L., 2012. Study of the Precambrian BIF-iron deposits in the North China Craton: progresses and questions. Acta Petrologica Sinica 28, 3431–3445.

Zhang, Y., Gu, X.X., Li, Y.H., Dong, S.Y., Cheng, W.B., 2010. Element geochemical characteristics of the Wangjiazhuang banded magnetite-quartzite deposit in Yuanping City, Shanxi Province, and its geological significance. Geoscience 24, 69–79.

Zhao, G.C., Cawood, P.A., Lu, L.Z., 1999. Petrology and P–T history of the Wutai amphibolites: implications for tectonic evolution of the Wutai Complex, China. Precambr. Res. 93, 181–199.

Zhao, G.C., Kröner, A., Wilde, S.A., Sun, M., Li, S.Z., Li, X.P., Zhang, J., Xia, X.P., He, Y.H., 2007. Lithotectonic elements and geological events in the Hengshan–Wutai–Fuping belt: a synthesis and implications for the evolution of the Trans-North China Orogen. Geol. Mag. 144, 753–775.

Zhao, G.C., Li, S.Z., Zhang, J., Sun, M., Xia, X.P., 2010. A comment on "Tectonic evolution of the Hengshan–Wutai–Fuping complexes and its implication for the Trans-North China Orogen". Precambr. Res. 176, 94–98.

Zhao, G.C., Sun, M., Wilde, S.A., Li, S.Z., 2005. Late Archean to Paleoproterozoic evolution of the North China Craton: key issues revisited. Precambr. Res. 136, 177–202.

Zhao, G.C., Wilde, S.A., Cawood, P.A., Sun, M., 2002. SHRIMP U–Pb zircon ages of the Fuping Complex: implications for Late Archean to Paleoproterozoic accretion and assembly of the North China Craton. Am. J. Sci. 302, 191–226.

Zhao, G.C., Zhai, M.G., 2013. Lithotectonic elements of Precambrian basement in the North China Craton: review and tectonic implications. Gondwana Res. 23, 1207–1240.

Zhao, R.F., 2012. Petrogenesis of late Archean TTG gneisses and Paleoproterozoic potassic granites in Hengshan terrane, North China Craton. Doctoral Dissertation, University of Chinese Academy of Sciences, p. 143.